

Deployment of Energy-Efficient Deep Learning Models on Cortex-M based Microcontrollers using Deep Compression

Mark Deutel¹, Philipp Woller², Christopher Mutschler², and Jürgen Teich⁴

Abstract—Large Deep Neural Networks (DNNs) are the backbone of today’s artificial intelligence due to their ability to make accurate predictions when being trained on huge datasets. With advancing technologies, such as the Internet of Things, interpreting large quantities of data generated by sensors is becoming an increasingly important task. However, in many applications not only the predictive performance but also the energy consumption of deep learning models is of major interest.

This paper investigates the efficient deployment of deep learning models on resource-constrained microcontroller architectures via network compression. We present a methodology for the systematic exploration of different DNN pruning, quantization, and deployment strategies, targeting different ARM Cortex-M based low-power systems. The exploration allows to analyze trade-offs between key metrics such as accuracy, memory consumption, execution time, and power consumption. We discuss experimental results on three different DNN architectures and show that we can compress them to below 10% of their original parameter count before their predictive quality decreases. This also allows us to deploy and evaluate them on Cortex-M based microcontrollers.

Index Terms—Deep Neural Networks, Deep Compression, Network Pruning, Weight Quantization, Microcontrollers

I. INTRODUCTION

DEEP Neural Networks (DNNs) became predominant in many applications that require autonomous decision-making based on environmental information, including audio recognition [1], [2], image classification [3], [4], or human activity monitoring [5]. DNNs are beneficial as they are easy to set up and as they can be trained to detect correlations even when they are confronted with high-dimensional data.

However, the execution of DNNs is energy-, resource-, and time-expensive [6], [7]. In situations where the trade-off between resource constraints, execution time, and predictive quality is key, DNNs often struggle to compete with classical machine learning approaches [8]. However, with trends like *smart devices* and the *internet of things* (IoT), the demand and interest in deploying DNNs on microcontrollers grows.

Deep compression is a relatively young research area that deals with the compression of DNNs. Prominent techniques include DNN graph pruning [9], weight quantization [10],

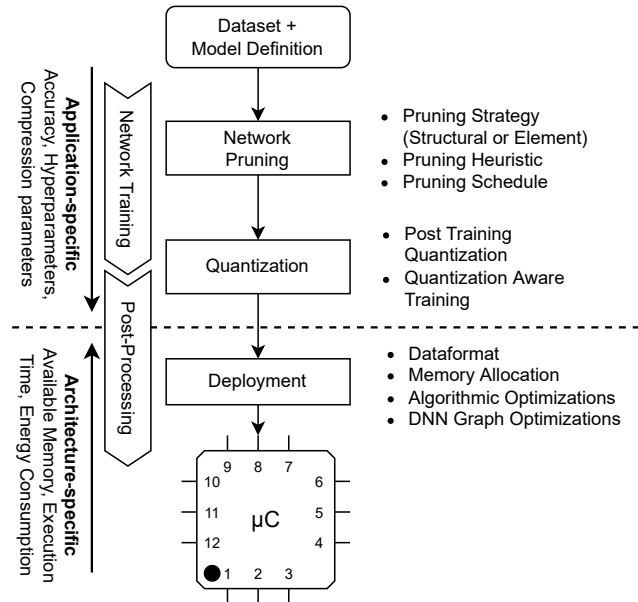


Fig. 1. Overview of our methodology.

[11], and subspace methods [12]. Their goal is to reduce the resource footprint of a DNN by reducing the number of trainable weights and computational complexity while preserving the original predictive performance.

Based on these principles different DNN compression pipelines have been proposed. Most noticeably, Han et al. [13] who proposed a pipeline combining network pruning, integer quantization, and Huffman encoding. Others focus on quantization during network training [10] or on structure-based pruning. This allows for an immediate removal of pruned weights [14], [15]. However, such well-established frameworks only trade compression over predictive accuracy but do not explicitly target energy-efficiency and architecture-specific constraints like memory availability and processing speed that play an important role in many embedded applications.

This paper proposes a methodology to systematically train and deploy DNN architectures on Cortex-M-based microcontrollers. We introduce an automated pipeline that covers application-specific DNN training and compression, and that combines it with a target architecture-specific deployment, see Fig. 1. Our proposed pipeline is composed of two major building blocks. First, from an application-specific viewpoint we systematically explore compression techniques, i.e., network pruning and weight quantization, and configurations during

¹ Mark Deutel is with Fraunhofer IIS, Fraunhofer Institute for Integrated Circuits IIS, Nuremberg, Germany and Friedrich-Alexander-Universität Erlangen-Nürnberg (FAU), Erlangen, Germany mark.deutel@fau.de

² Phillip Woller and Christopher Mutschler are with the Fraunhofer IIS, Fraunhofer Institute for Integrated Circuits IIS, Nuremberg, Germany firstname.lastname@iis.fraunhofer.de

³ Jürgen Teich is with Friedrich-Alexander-Universität Erlangen-Nürnberg (FAU), Erlangen, Germany juergen.teich@fau.de

the training of DNNs. Second, incorporating an architecture-specific view, we realize the mapping from a high-level graph-based DNN representation to low level code. This step involves an offline code generator and a runtime library. The former takes care of the data layout, plans memory allocation and emits executable code while the latter provides implementations of common DNN layers used by the generated code. Novel methods implemented in our proposed pipeline include ahead-of-time code generation and memory allocation scheduling, which eliminates the need for any form of network interpretation or dynamic memory management at runtime, and the exploitation of sparse matrices generated as part of our pruning techniques using the *Compressed Column Storage (CCS)* format [16].

In our experiments we evaluate both compression and deployment for three common DNN architectures, i.e., AlexNet [17], ResNet [3] and LeNet [18]. Our objective is a thorough evaluation of the relation between compressed DNNs and their predictive quality. In contrast to previous work our results do not only focus on deployment or compression alone, but provide detailed insight into the relationship between different pruning, quantization, and deployment strategies when applied in combination. Furthermore, we deployed the compressed models on three target systems and discuss their memory consumption, execution time, and power consumption.

The rest of this paper is structured as follows. Sec. II discusses related work. Secs. III and IV provide details about our compression and deployment pipeline. Sec. V discusses our experimental results. Sec. VII concludes.

II. RELATED WORK

Existing research predominately compresses DNNs via network pruning and weight quantization. These techniques are well understood as research has been conducted exploring the effects of pruning and quantization on a network's predictive performance [19], [20]. However, when deploying applications for embedded targets, they are defined by the constraints imposed by the platforms they use. As a result, the suitability of DNN models for deployment on microcontrollers is not only determined by their accuracy but also by their memory footprint and inference time. Therefore, this work extends existing findings by analysing the effects of DNN compression not only on accuracy but also on relevant deployment metrics, i.e. memory consumption, latency, and energy consumption.

Furthermore, research that focuses on the deployment of DNNs to microcontrollers is often published in an application-oriented way, e.g., to realize real-time drowsiness detection [21] or to perform motor fault diagnosis [22]. Those platforms do not serve as general purpose frameworks as they are tightly optimized to the particular application requirement and as they do not generalize to a broader set of target architectures.

Nevertheless, recent scientific work has provided some insight into generalized deployment of DNNs on microcontrollers. The approach most closely related to our proposed methodology is MCUNet [23]. Similar to our pipeline the authors describe a two stage process to seamlessly combine model design (TinyNAS) with an inference engine

(TinyEngine). Still MCUNet differs from our approach in the way it generates suitable DNN candidates for deployment. To find networks that meet target platform constraints, MCUNet focuses on neural architecture search (NAS) [24] while our framework starts from well-known existing DNN architectures and then dynamically scales them down during their training using pruning and quantization techniques.

A more general approach to a deployment framework for microcontrollers is *tfl-micro* [25], which supports the execution of quantized tensorflow lite models on ARM Cortex-M-based hardware using ARM's *CMSIS* library. However, this also limits the framework as it requires the usage of *tensorflow (TF)* for model training and also only supports a subset of features implemented in TF.

Besides that there are also commercial frameworks focusing on embedded platforms. Noticeable examples are STM's *X-CUBE-AI*¹, that allows for the automatic conversion of pre-trained AI algorithms to deployable code as well as web-service based end-to-end solutions like *Edge Impulse*² or *SensiML*³. However, such commercial frameworks are often either black boxes (e.g., X-CUBE-AI) or they base themselves on already existing underlying solutions (e.g., *Edge Impulse* uses *tfl-micro*) and their limitations.

III. COMPRESSION AND DEPLOYMENT PIPELINE

Our pipeline is fully integrated and seamlessly covers the complete DNN training and deployment process. Our methodology uses both network pruning (Sec. III-A) and weight quantization (Sec. III-B) which can both be controlled via a set of additional *hyperparameters*. Furthermore, the trained and compressed DNNs are directly converted from their graph-based representation to executable architecture-specific program code (see Sec. IV). As a result, our pipeline can easily be integrated with existing meta-heuristic optimization frameworks (e.g. Optuna [26]) to conduct automated design space exploration.

A. Network Pruning

Our pipeline implements configurable elements for network pruning, i.e., (1) pruning techniques, (2) pruning heuristics, and (3) pruning schedule. which we describe in the following.

Pruning techniques. Pruning DNNs by removing parameters has been proposed early [9], [27]. While initially being introduced to improve generalization and convergence it recently became a standard size reduction technique with no or low cost of accuracy. Our pipeline implements *element-wise pruning* and *structural pruning*. Element-wise pruning removes connections from a DNN's compute graph, i.e., parameters of the network are set to zero. Hence, these parameters do no longer influence the training error and are removed from the scope of the optimizer that trains the network. Structural pruning sets whole structures of parameters to zero. This has shown to be very efficient for pruning filters [14] or channels [15] of 2D-convolutional layers but it can analogously also be applied to

¹<https://www.st.com/en/embedded-software/x-cube-ai.html>

²<https://www.edgeimpulse.com/>

³<https://sensiml.com/>

rows and columns of linear layers. Its major benefit is the removal of complete structures from the weight tensors at once, which results in a considerable immediate reductions of parameters (which is in contrast to element-wise pruning that only creates sparse weight tensors).

Pruning heuristics. A critical aspect of pruning is the selection of elements or structures that, when removed, have the least impact on predictive performance. Oracle pruning [28] finds an optimal selection by removing every single structure and element of a network before evaluating its impact on the prediction quality. In practical applications this approach cannot be applied as it is too resource- and time-consuming. Fortunately, there have been proposed a number of heuristics that approximate optimal element-wise or structural pruning. In our framework we implemented many popular approaches that are based on different criteria such as magnitude [29], L-norm [14], gradient [28] or percentage of zeros found in activations [30] to rank parameters or parameter structures by their approximated importance.

Pruning schedules. The pruning schedule determines when, how often, and to what extent a DNN will be pruned during training. We implement two well-known approaches: *One-Shot Pruning* [9] and *Iterative Pruning*. One-shot pruning first trains a DNN until it achieves a *reasonable* accuracy on the test dataset, and then prunes the DNN (optionally followed by a few epochs of re-training). Iterative pruning prunes a DNN over the course of training, which allows for an interleaved re-training. Hence, not all weights are removed at the same time but step by step over several pruning iterations (finally enforcing maximal sparsity). We implemented *Automated Gradual Pruning (AGP)* [31], which gradually increases the number of pruned weights s_t starting at t_0 from an initial sparsity s_i to a final sparsity s_f over n steps:

$$s_t = s_f + (s_i - s_f) \left(1 - \frac{t - t_0}{n\Delta t}\right)^3, \quad t \in \{t_0, \dots, t_0 + n\Delta t\}. \quad (1)$$

B. Weight Quantization

Quantization reduces the numerical resolution of the parameters and their computation. This not only cuts down the memory footprint but also the computational complexity of a DNN. However, as parameter quantization comes with an additional error on the predictive performance a major challenge lies in the selection of a good trade-off between predictive quality and parameter resolution.

Our framework uses an *affine mapping* scheme that transforms an original floating-point parameter into an 8-bit unsigned integer⁴. We apply a function $f(x)$ in combination with additional sets of trainable scale and zero point parameters:

$$f(x) = g\left(\left\lfloor \frac{x}{s} \right\rfloor + zp\right), \quad (2)$$

$$s = \frac{\max_{data} - \min_{data}}{255}, \quad 0 \leq zp \leq 255,$$

where $g(x)$ is the clamp-function to avoid data type overflows:

$$g(x) = \begin{cases} x & \text{if } 0 \leq x \leq 255 \\ 255 & \text{if } x > 255 \\ 0 & \text{if } x < 0. \end{cases} \quad (3)$$

The scale parameter s defines the step size of the quantization, which is calculated as the ratio between the span in which values are distributed in the original floating-point space and the span covered by the quantized integer space. The zero point parameter zp denotes an exact point in quantization space that represents zero in the original floating-point space. The two parameters can be defined either per tensor or per structure.

Quantization can not only be applied to weight tensors but also to activation tensors. We refer to this as *full integer quantization*. During execution most computations can then be performed in integer instead of floating-point space which is beneficial for target systems that are not equipped with floating-point units. We give an example for applying full-integer quantization to matrix-multiplications. The general form is defined as:

$$c_{ij} = \sum_{k=0}^n a_{ik} \cdot b_{kj}, \quad \forall i \in \{0, \dots, m\}, \forall j \in \{0, \dots, p\}, \quad (4)$$

where the first line describes how the elements of a matrix C are calculated from the elements of a $m \times n$ matrix A and a $n \times p$ matrix B . In a fully-quantized DNN, both matrices A and B contain integer values and we first must de-quantize them by rearranging Equation 2 before we multiply them. As the resulting matrix C is represented in the un-quantized space, we have to quantize it by applying Eq. 2 again. By substituting and rearranging the previous computations we obtain

$$c_{ij} = g\left(zp_c + \left\lfloor \left(\frac{s_a \cdot s_b}{s_c}\right) \sum_{k=0}^n (a_{ik} - zp_a)(b_{kj} - zp_b) \right\rfloor\right). \quad (5)$$

Note that only the scale parameters $\{s_a, s_b, s_c\} \in \mathbb{R}$ while all other parameters $\in \mathbb{N}_0$.

Our pipeline implements two popular ways of determining at which point quantization is applied to a DNN. The first method quantizes as a post process (PPQ) [11], [33], i.e., after training has finished, and the second method integrates quantization into the training loop. The latter is denoted by *Quantization-aware Training (QAT)* [10]. Both techniques come with their advantages and disadvantages: PPQ is extremely easy to integrate as it can be performed completely decoupled from a DNN's training process and does not requires any invasive changes to a DNN's architecture (i.e., no re-training to fine-tune quantization parameters). However, this usually comes at the cost of a larger error introduced by quantization as the required scale and zero point parameters are only roughly approximated. In contrast, QAT adapts quantization parameters as part of a DNN's training process and can hence yield better results. However, QAT only works properly with extensive network augmentation, which leads to a more complex and computationally expensive training process.

IV. ARCHITECTURE-SPECIFIC DEPLOYMENT

Our pipeline provides a deployment framework for targeting microcontrollers, see Fig. 2. We call this framework *dnnrun-*

⁴See also [32] and <https://onnruntime.ai/docs/how-to/quantization.html>.

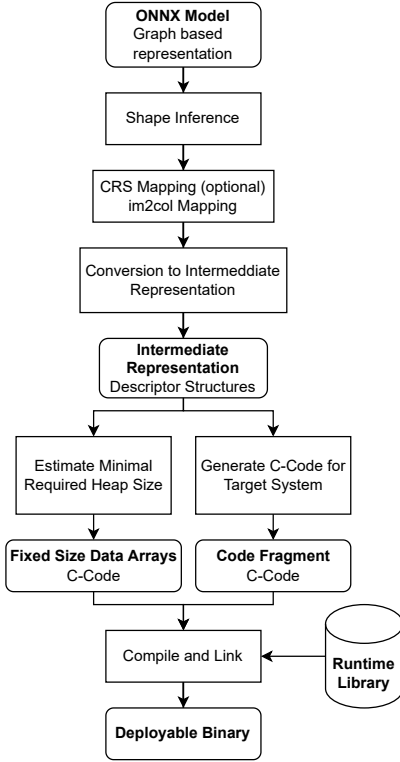


Fig. 2. Overview of the process implemented by our conversion tool, mapping trained ONNX DNN models to C-Code and finally compiling them to deployable binaries.

time. It uses a platform-independent, offline, and ahead of time conversion tool together with a runtime library. The conversion tool maps pre-trained DNNs stored in the ONNX format to C code (Sec. IV-A), while the runtime library implements platform-specific DNN operators that are subsequently used by the code emitted from the conversion tool (Sec. IV-B). Our implementation is novel in the way that it exploits static properties of trained DNNs (i.e. fixed layer configurations and parameters), and therefore removes the necessity of interpreting the DNN at runtime. This includes dynamic allocation of memory for intermediate tensors which can be simulated offline allowing heap allocation to be conducted at compile time. This not only decreases the computational overhead at runtime but also allows metrics like simulated memory consumption to be directly fed back into the overall optimization process without having to evaluate the model on the target system.

A. Conversion Tool

The main functionality of the conversion tool is to generate ANSI C code based on a given ONNX model of the DNN to be deployed. This involves two steps: (1) parsing and converting the model to an intermediate representation, and (2) using this representation to determine a suitable data format, simulate memory allocation and generate an implementation describing the model’s structure in code.

The ONNX format stores a DNN’s compute graph as a directed, acyclic graph with a set of fixed inputs and outputs. Every node in the graph represents an operation and can

$$A = \begin{bmatrix} 10 & 0 & 0 & 0 & 1 \\ 0 & 7 & 0 & 2 & 0 \\ 0 & 0 & 8 & 0 & 0 \\ 14 & 0 & 0 & 0 & 6 \end{bmatrix}$$

values	10	1	7	2	8	14	6
col_ind	0	4	1	3	2	0	4
row_ptr	0	2	4	5	7		

Fig. 3. Conversion of an asymmetric matrix A (left) into its CRS representation (right): we emit three smaller arrays to the bytes-stream instead of one. The first one contains all non-zero values, the second one contains column indices, and the third one contains row pointers.

have multiple incoming and outgoing edges assigned to it. Edges describe the dataflow during the DNN’s execution. Besides that, based on the type of operation a node represents, additional static parameters tensors can also be assigned to it.

1) *Mapping ONNX to target-specific intermediate format*: We first map a given ONNX representation to an architecture-specific intermediate format that can be used to emit program code later on. This involves three consecutive steps.

First, we concatenate the static tensors of all nodes into a byte-stream. The single elements of each tensor are stored in the stream by using a little-endian byte order as this is the default memory format on ARM architectures (of course, this can be modified easily). Additionally, we add padding bytes where necessary to avoid triggering the memory protection unit (MPU) when accessing tensor data at runtime. Afterwards, we generate descriptor structures containing the location of each tensor in the byte-stream and additional metadata such as data types and tensor shapes. Sparse tensors are handled as edge cases as they are generated by element pruning during our pipeline’s compression stage. To reduce memory usage, our tool applies a conversion from the original full-sized layout of the tensors to a more compact *Compressed Row Storage (CRS)* [16] layout, see Fig. 3 for an example. CRS reduces the memory footprint, allows for an optimized implementation of matrix-vector products, and does not pose any requirements on how sparsity is distributed inside a tensor (hence, element pruning during compression can ignore the subsequent space-saving storage of pruned tensors). A disadvantage of CRS is that it can only be applied to 2D-tensors (matrices), which means that we need to map higher dimensional weight tensors of convolutions to 2D space before processing them.

Second, the conversion tool generates descriptor structures for all dynamic activation tensors. This is more complicated than it is for static parameter tensors as activation tensors are only represented in the ONNX model’s compute graph as edges. Edges are not required to provide any meta information like data types or shapes. However, this information is mandatory for our conversion tool. Hence, we implement a process called *shape inference*. The idea is to trace the execution of a DNN through its compute graph from input to output nodes, and to use these traces to infer the shapes and types of intermediate tensors assigned to inner edges.

Third, we parse and interpret all operator nodes in the ONNX compute graph and bring them into a topological and serialized order. This information is then used during code generation to determine the execution order of operations.

2) *Code Generation*: Using the intermediate representation generated by the first step the conversion tool can emit code. We start by estimating the minimal heap size required for

storing activation tensors. This information can be queried offline as once the training of a DNN is complete, its structure and dimensionality remains unchanged throughout its lifetime. Using the minimal heap size, we define a fixed-size memory balloon at compile time (eliminating the need for dynamic memory management at runtime). A naive approach that estimates the size of this balloon calculates the product of the shapes of all activation tensors and multiplies them with the byte sizes of their respective data types. However, this is not space-efficient as usually the lifetimes of these tensors are rather short. Hence, parts of the heap memory can be reused for multiple tensors during an inference pass. This may have a big impact on the amount of memory required.

We take advantage of this by implementing an offline *memory planning algorithm* based on graph tracing and using a first-fit allocation strategy therein. We estimate optimal heap re-usage in two steps: First, based on incoming and outgoing edges of nodes (i.e., operators) in the input model, the algorithm creates two lists per operator: The first list contains all tensors that have to be allocated for that operator (i.e., allocation list) and the second list contains all previously allocated tensors that can be discarded (i.e., release list). Second, the algorithm proceeds iterating through the sequence of operators starting with an empty, infinitely sized memory balloon. For each operator, it first iterates the tensors in the corresponding free list and marks their space in the memory balloon as unoccupied. After that, it iterates the allocate list and tries to reserve pieces of memory based on the shapes and data types of the tensors. To find suitable locations in the balloon, the algorithm compares the required sizes with available segments of free memory starting from the beginning (i.e., first fit). Once it found suitable pieces of memory, it marks them as allocated in the balloon and stops searching. During all steps, the algorithm keeps track of the maximum size of the memory balloon.

The emitted code implements a two-function API: The first function allows to setup the converted DNN and the second function executes an inference given an input sample. The latter is implemented based on the list of topologically sorted ONNX operator nodes stored in the previously generated intermediate representation. For each operator a function call is emitted. These functions are implemented by the *runtime library*. To give context to these function and pass intermediate results between them, we provide references to constant tensor descriptor structures generated as part of the intermediate representation. All static data associated with weight tensor descriptors is stored in a byte-array in the intermediate representation. Therefore, a constant C-array (i.e. flash memory) containing all the data is emitted, accordingly.

The amount of random access memory required for intermediate activation tensors is based on the minimal memory balloon previously estimated by our *memory planning algorithm*. Hence our tool emits another accordingly sized zero initialized non-constant C-array (i.e. heap memory).

B. Runtime Library

To perform the operations described by the input ONNX model, the code emitted by our conversion tool relies on

additional DNN operator functionality that we implement by a runtime library. Currently, this includes operators such as convolutions, linear transformations, batch-normalization, pooling operations, and activation functions. All our implementations follow the ONNX operator specification⁵. Where required, we also implement quantized versions of these operators.

Based on the target platform there are different possibilities to optimize the execution of DNNs. During profile tests we found that most execution time is spent on computing convolutions or matrix-vector products. Hence, an optimal implementation of these operator types yields significant improvements in both resource consumption and execution time. Less crucial but still significantly, some operations can be removed from a DNN’s compute graph by applying graph optimization, which we apply after DNN training and compression. Notable optimization techniques include *batch normalization folding* [10] and the fusing of ReLU activation functions into preceding quantized linear or convolutional operations [10].

For our experiments we focus on Cortex-M0+ and Cortex-M4 processors. This is why our implementation heavily makes use of the information of these processor architectures. A major algorithmic optimization that we apply is to unroll 2D convolutions into more CPU- and memory-friendly matrix-vector products (*im2col mapping*). Hence, during mapping we rearrange both the input tensors and the parameter tensors of convolutions. This is a common approach used in digital signal processing.⁶ In addition, this mapping also enables our conversion tool to apply CRS to convolutional layers.

Since DNNs also use matrix-vector products in linear transformations, a nice additional side-effect is that by using the *im2col* mapping complete inference passes can be described by matrix-vector products and non-linearities alone. Moreover, ARM provides optimized open-source implementations for matrix products in their *CMSIS* library⁷. Using them is especially beneficial on architectures like the Cortex-M4 as it allows to use SIMD instructions provided by ARM’s *Digital Signal Processing (DSP)* extension, see Sec. V.

V. EVALUATION

To evaluate our pipeline we selected three popular DNN architectures: (1) a convolutional network similar to the one proposed by Krizhevsky et al. [17] to classify CIFAR-10 images (AlexNet), (2) a residual network [3] (ResNet), and (3) a smaller network architecture initially proposed by LeCun et al. [18] (LeNet) for classifying the MNIST handwritten digit database. See Table I for more details.

We trained AlexNet and ResNet on the CIFAR10 [4] dataset for 100 epochs with mini-batches of size 80 and LeNet on the MNIST handwritten digit datasets [34] for 20 epochs with mini-batches of size 48 (as training converges on MNIST considerably faster). On all the models we used stochastic gradient descent (SGD) with a momentum of 0.9 and a learning rate of $1e - 3$. We achieved a maximum accuracy

⁵<https://github.com/onnx/onnx/blob/master/docs/Operators.md>

⁶e.g., Matlab® provides `convmtx()` and `convmtx2()` for this task.

⁷https://github.com/ARM-software/CMSIS_5

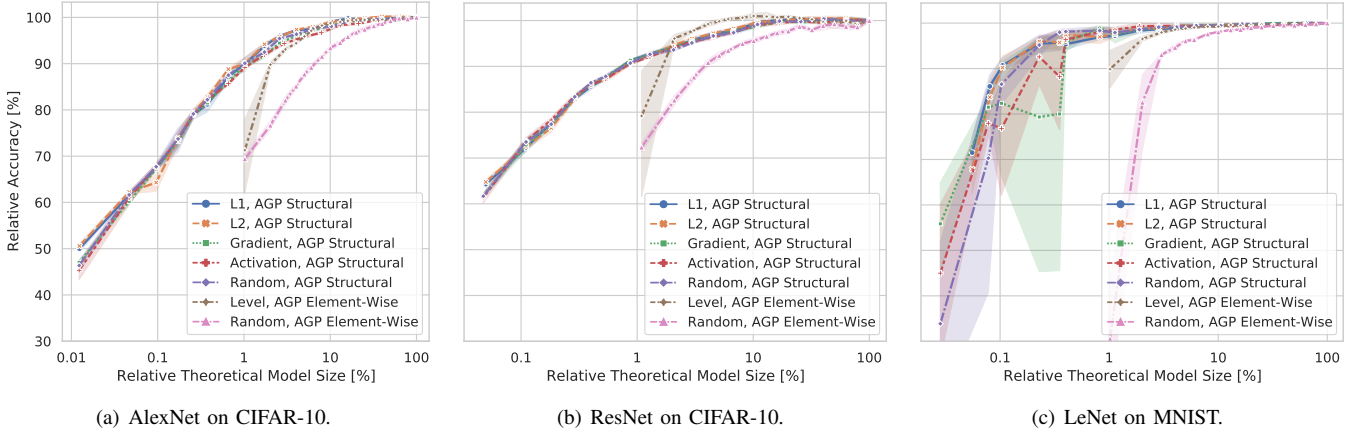


Fig. 4. Element-wise and structural pruning applied to the DNN architectures. The curves describe the relation between theoretical model size and accuracy of compressed models relative to their uncompressed baselines when using different pruning techniques in combination with an iterative AGP pruning schedule. We define theoretical model size to be the number of weights a model features excluding all weights that have been set to zero by pruning.

TABLE I
PARAMETERS OF THE DNN ARCHITECTURES USED IN OUR EXPERIMENTS.

AlexNet (44.7M)	ResNet (9.4M)	LeNet (1.2M)
<i>Input:</i> [3, 32, 32]		<i>Input:</i> [1, 28, 28]
[3, 64, 2, 2]	[64, 64, 3, 1]	[1, 32, 3, 1]
[64, 192, 3, 1]	[64, 128, 3, 1]	[32, 64, 3, 1]
[192, 384, 3, 1]	[128, 256, 3, 1]	
[384, 256, 3, 1]	[256, 512, 3, 1]	
MaxPool: [2]		
[6400, 4096]	[25088, 10]	[9216, 128]
[4096, 4096]		[128, 10]
[4096, 10]		
<i>Output:</i> [10]		
SoftMax		

Tuples describe linear layers in the form of [num. inputs, num. outputs]. Every layer uses ReLU as their non-linearity except the last ones which are followed by SoftMax; AlexNet/LeNet: quadruples describe 2D-convolutions by [channels, filters, kernel size, stride]; ResNet: quadruples describe residual blocks each with two 2D-convolutions in the form of [block in. channels, block out. filters, conv. kernel size, conv. stride]; AlexNet/ResNet: every 2D-convolution is followed by batch normalization.

TABLE II
MICROCONTROLLERS CONSIDERED IN OUR EVALUATION.

	Raspberry Pi Pico	Arduino Nano 33 BLE Sense	Raspberry Pi 4B
Processor	RP2040, Cortex-M0+ (Armv6-M)	nrf52840, Cortex-M4 (Armv7-M)	BCM2711 SoC, Cortex-A72 (Armv8-A)
Clock	133 MHz	64 MHz	1.5 GHz
Flash	2 MB	1 MB	16 GB (SD-Card)
RAM	256 KB (SRAM)	256 KB (SRAM)	8 GB (SDRAM)
SIMD	No	Yes (ARM DSP)	Yes (ARM Neon)

of 86.51% for AlexNet, 85.97% for ResNet, and 98.46% for LeNet that serve as baselines for our experiments.

To evaluate our deployment pipeline we selected three target systems: (1) a Raspberry Pi Pico, (2) an Arduino Nano 33 BLE Sense, and (3) a Raspberry Pi 4B (that serves as a larger reference system), see Table II. As our runtime library is

mainly optimized for Cortex-M architectures, we instead use onnxruntime [32] for the deployment to the Raspberry Pi 4B.

We compare the performance of different pruning techniques in Sec. V-A and discuss their combination with quantization in Sec. V-B. We analyze the memory footprint of our compressed DNNs in Sec. V-C. In Sec. V-D we discuss the execution time and power/energy consumption w.r.t. the predictive accuracy from a real-world execution of the compressed DNNs on the target platforms.

A. Comparison of Pruning Techniques

First, we present results of pruning experiments conducted for each of our three test DNN architectures. We repeated model training from scratch and increased pruning target rates starting with 0% as the un-pruned baseline and ending with 99% (i.e., a relative theoretical model size of 1%) as the most aggressively pruned configuration. For each of the configurations we repeated the experiment five times and report their means and standard deviations.

Figs. 4 and 5 show the predictive accuracy of the models (relative to the un-pruned baseline) over percentages of theoretically remaining parameters on the validation dataset. We first investigate the influence of pruning schedules on

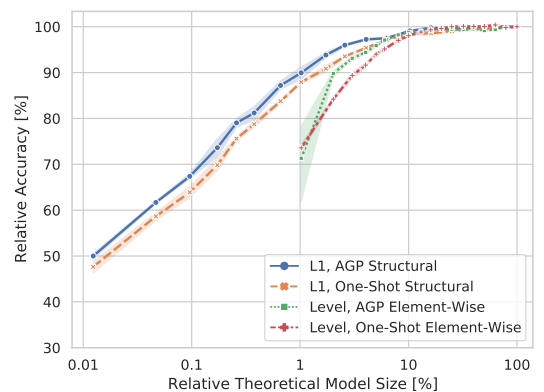


Fig. 5. Comparison of pruning schedules for both structural and element-wise pruning with AlexNet on CIFAR-10 (L1: pruning selected parameters based on ℓ_1 -norm; Level: selects parameters based on magnitude level).

the achievable pruning rate, see AlexNet on CIFAR-10 in Fig. 5. While we cannot observe major differences between *iterative* (i.e., Automated Gradual Pruning, AGP) and *one-shot* schedules for final parameter counts $> 10\%$, we see that iterative schedules perform slightly better both for element-wise and structural pruning for parameter counts below 10% . We argue that this is because it is more difficult for the network to retrain when a large number of parameters are removed at once than when parameters are removed gradually and retraining is possible in between. Hence, we decided to focus on iterative pruning schedules for all further experiments.

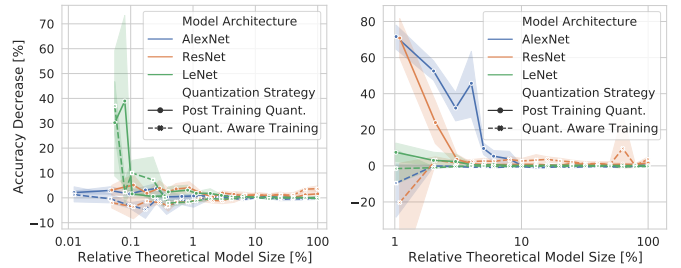
With the iterative AGP schedule on the same experimental setup we tested different pruning heuristics for structural and element-wise pruning on all architectures, see Figs. 4(a) to 4(c). We report four different heuristics for structural pruning and one for element-wise pruning alongside a random selection ('Random') approach as a baseline for the more elaborate heuristics. For structural pruning, we use both the ℓ_1 - and the ℓ_2 -norm of parameter structures ('L1' and 'L2') as well as their gradient size ('Gradient') and the average percentage of zeros in their corresponding activation ('Activation') as heuristics. For element-wise pruning we use a magnitude level to decide which elements to prune ('Level').

While we see a significant improvement of the level-based heuristic over the corresponding random selection for element-wise pruning on all our three DNN architectures, we cannot observe a similar behaviour for structural pruning. Instead, none of the more complex structural pruning heuristics managed to significantly improve over the random selection approach. There is also only little variation in the results of the heuristics. We believe that the main reason for this is the iterative re-training between pruning steps: while introducing pruning during DNN training can cause degradation in the predictive quality of a model, it was very often regained in a short number of epochs when re-training. This is in line with results reported in previous work [29].

In all our experiments we used the same target compression rates for both element-wise and structural pruning. However, we see that the structural pruning experiments resulted in models that exceed their selected targeted compression rate. In some cases this reduces the parameter count to almost 99.9%. For element-wise pruning, we do not see such an effect. The reason for this is related to the removal of structures from DNN models during structural pruning: due to the existence of data dependencies between layers, removing structures from their parameter tensors also influences the shapes of tensors in surrounding layers. For element-wise pruning, parameters are not completely eliminated from the DNN but are instead just set to zero. Therefore, all data dependencies remain in the network, no tensor shape changes occur, and the pruning target rate is more precisely met.

B. Combining Pruning and Quantization

We present experimental results for weight quantization in combination with pruning for our three test DNN architectures. Fig. 6(a) shows the results for quantization in combination with structural pruning and Fig. 6(b) shows the results for



(a) L1-norm AGP structural pruning (b) Level AGP element-wise pruning

Fig. 6. Decrease in accuracy on the evaluation dataset observed for our three DNN architectures when combining pruning and quantization techniques.

element-wise pruning. The different colors refer to the models we trained and quantization strategies are differentiated with the line and marker style. We aim to give an understanding on how much the additional quantization error alone influences the prediction quality of quantized models. Hence, as before, the x -axes show the relative theoretical model size reduction while this time the y -axes reports the accuracy decrease of each pruned and quantized model in relation to its pruned but not quantized version.⁸ This allows us to focus on the additional error that is introduced through quantization alone.

When looking at the results of structural pruning in combination with both Quantization as a post process after training (PPQ) and Quantization Aware Training (QAT), we see that the techniques work well together with pruning for all our three architectures. In Fig. 6(a) we see that the accuracy decrease consistently is $< 5\%$ even when using quantization in combination with aggressive pruning regimes. The only outliers we monitored were part of our experiments on the LeNet architecture. Here, for the two most aggressive pruning configurations, the accuracy decrease between the non-quantized and quantized models went to around 40% for both tested quantization strategies. Moreover, we observed an increase in standard deviation as accuracy decreased, which we believe is related to an increase in variance in the trained weight values that we observed for LeNet at higher compression rates. The higher the variance of the values in a weight tensor, the worse quantization can represent these values in integer space.

We also tested element-wise pruning in combination with PPQ and QAT, see Fig. 6(b). Other than for structural pruning, where PPQ performed consistently well even in combination with aggressive pruning configurations, for element-wise pruning we observed accuracy decreases of over 70% in comparison to the un-quantized versions. In particular, we observe that PPQ noticeably failed for models that have been compressed by element-wise pruning to 10% or less of their original parameter count. This is despite the fact that the technique performed well for pruning configurations that target compression rates above 10%. In contrast, QAT performed significantly better than PPQ even when used together with aggressive pruning configurations. The technique was able to

⁸We want to point out that quantization does not change the number of parameters in a model, only their resolution, so the application of quantization does not affect the relative theoretical model size, although the model effectively becomes smaller. We present our findings on actual size reduction achievable with quantization in Sec. V-C.

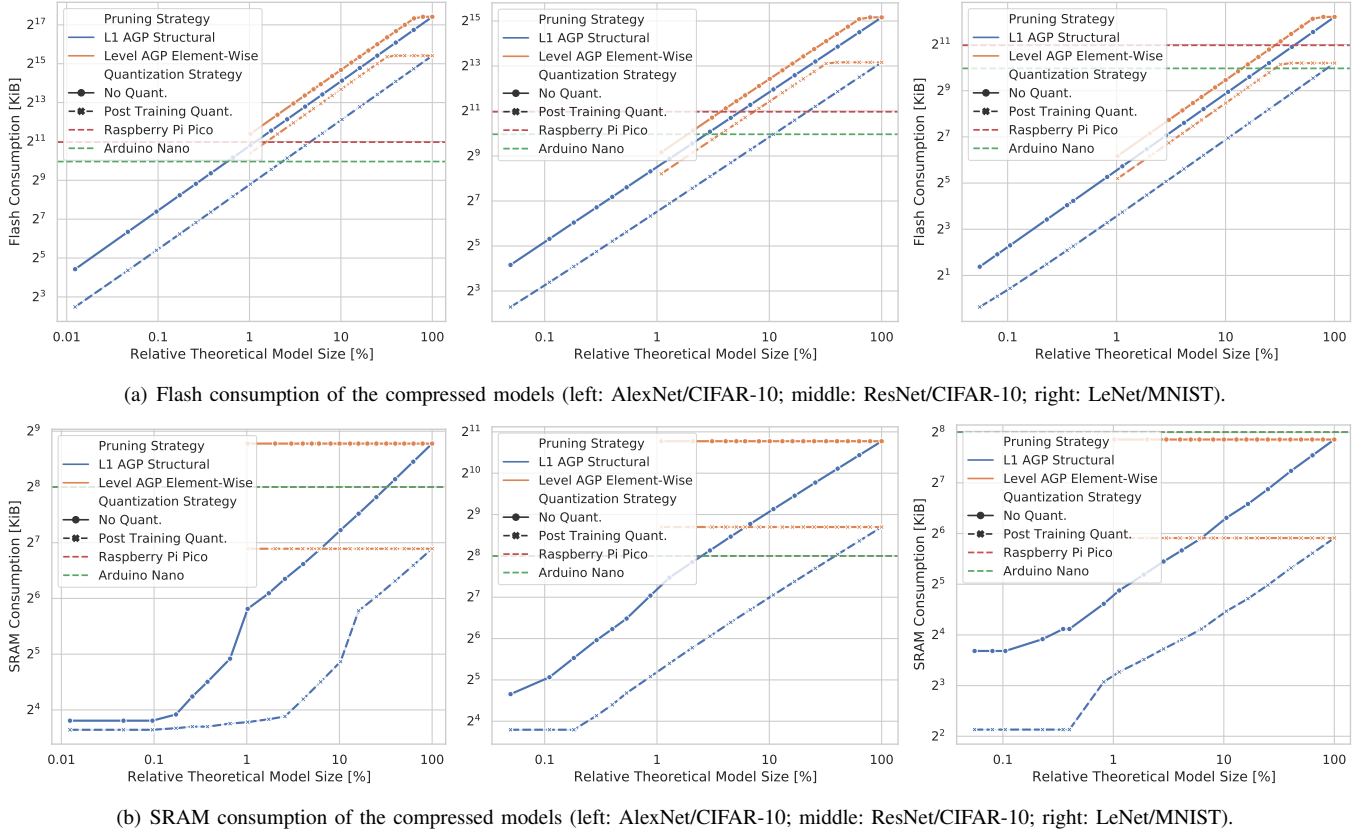


Fig. 7. Memory required for the deployment of our three DNN architectures (AlexNet, ResNet, LeNet) when applying the proposed runtime environment. (a) shows the required amounts of read-only “Flash” memory to store the DNNs’ trained weights, while (b) shows the required amounts of random access memory “SRAM” to store the dynamic activation tensors. The dashed horizontal red and green lines mark the memory limits of our two considered embedded target platforms, the Raspberry Pi Pico and the Arduino Nano 33 BLE Sense.

keep the accuracy decrease very close to 0% during all conducted experiments. Hence, we conclude that PPQ generally seems to perform better when being applied in combination with structural pruning than when used with element pruning. QAT on the other hand performed consistently well, both in combination with structural and element-wise pruning.

C. From Size Reduction to Memory Consumption

As described in Sec. IV the execution of DNNs requires both static read-only and dynamic random access memory. We now discuss the memory footprint of the models when they are being deployed. Fig. 7(a) shows the relation between relative model size (on the x -axes) and ROM/flash consumption in Kibibyte (on the y -axes) and Fig. 7(b) shows the same relation for SRAM. The curves for the pruned models are drawn with solid lines while the curves for the models where additional quantization was applied are dashed. To also highlight the importance of model compression we added the Flash and SRAM limits of our two microcontroller target platforms (red and green dashed horizontal lines). On both of these platforms flash and SRAM availability are two of the main bottlenecks for deployment.

We see a linear correlation between flash consumption and relative theoretical model size for structural pruning in Fig. 7(a) (note that both axes are in logarithmic scale). The reason for this is that pruned structures can be completely removed from the model which immediately decreases its

memory consumption in the process. For element-wise pruning, there is no such direct correlation. Instead, when looking at the orange curves in Fig. 7(a) we observe plateaus for higher theoretical model sizes. This is because pruning only generates sparse weight matrices. Our runtime environment utilizes compressed row storage (CRS) as a special decoding technique to store sparse weight matrices space-efficiently. However, a characteristic of the technique is that decoding a tensor will only result in memory savings after a certain percentage of sparsity has been reached. For any amount of sparsity below this threshold, it is better to just use the default memory layout where all elements are saved sequentially.

An additional observation we made is that for models that are compressed using quantization and element-wise pruning the threshold at which CRS becomes feasible is much higher than for just pruned models. Again, this is related to the properties of CRS decoding. Instead of all values, only values unequal to zero (or a zero point) are stored. To preserve their position in the original un-decoded matrix, the row and column indices of the values must be stored as well. For larger matrices, like they exist in DNNs, these indices usually require 16- or 32-bit integers to be stored correctly. Therefore, memory savings made by CRS can be considered as a trade-off between storing some elements and their indices versus storing all elements without any indices. When introducing sparsity into matrices with 32-bit floating point values, this quickly becomes a good trade-off. However, since quantized

TABLE III
 AVERAGE ($n = 8$) EXECUTION TIME, POWER AND ENERGY CONSUMPTION OBSERVED PER INFERENCE FOR COMPRESSED VERSION OF LENE_T TARGETING TWO RELATIVE ACCURACY LEVELS. THE BASELINE MODEL ACHIEVED AN ACCURACY OF $\approx 98\%$ FOR BOTH FLOAT AND UIN_T8.

rel. accuracy	compression	type	system	execution time (ms)	power (mW)	energy (mWs)
>99.00%	99.18%	structure, float	arduino	44.15 ± 0.03	141.14 ± 0.07	6.23 ± 0.01
			pico	184.28 ± 0.17	81.42 ± 0.42	15.00 ± 0.07
			pi4b	1.81 ± 0.55	3754.70 ± 284.92	6.65 ± 1.35
		structure, uint8	arduino	18.84 ± 0.04	101.06 ± 1.80	1.90 ± 0.03
			pico	50.06 ± 0.03	79.37 ± 1.03	3.97 ± 0.05
			pi4b	2.16 ± 0.60	3624.90 ± 272.88	7.68 ± 1.53
	95.00%	element, float	arduino	—	—	—
			pico	1004.77 ± 0.07	81.44 ± 0.10	81.82 ± 0.11
			pi4b	5.66 ± 1.39	3772.18 ± 263.01	21.00 ± 3.34
		element, uint8	arduino	360.95 ± 0.09	142.28 ± 0.10	51.36 ± 0.04
			pico	392.23 ± 0.07	84.82 ± 0.37	33.27 ± 0.15
			pi4b	5.10 ± 1.27	3673.70 ± 332.91	18.31 ± 3.04
>97.00%	99.7%	structure, float	arduino	22.48 ± 0.01	105.32 ± 0.27	2.37 ± 0.01
			pico	73.26 ± 0.33	81.72 ± 0.48	5.99 ± 0.03
			pi4b	1.91 ± 0.56	3554.33 ± 232.34	6.67 ± 1.48
		structure, uint8	arduino	18.79 ± 0.03	82.54 ± 0.80	1.55 ± 0.02
			pico	24.97 ± 0.44	79.92 ± 0.88	2.00 ± 0.04
			pi4b	2.01 ± 0.53	3581.79 ± 240.22	7.11 ± 1.41
	97.00%	element, float	arduino	—	—	—
			pico	658.70 ± 0.10	82.44 ± 0.68	54.30 ± 0.45
			pi4b	5.35 ± 1.23	3816.72 ± 246.08	20.12 ± 2.79
		element, uint8	arduino	303.15 ± 0.09	141.58 ± 0.05	42.92 ± 0.01
			pico	392.27 ± 0.10	84.67 ± 0.45	33.22 ± 0.18
			pi4b	4.64 ± 1.39	3787.84 ± 395.19	17.05 ± 3.16

values require only 8 bits, while the index values introduced by CRS are still usually at least 16 bits long, the amount of sparsity that has to be introduced before memory can be saved is higher.

Fig. 7(b) shows the relationship between relative theoretical model size and required SRAM. Similar to flash consumption, a correlation between model size and SRAM consumption can be observed for structural pruning. When structures are removed from parameter tensors during pruning, data dependencies between layers are also removed. Therefore, the shapes of the dynamic intermediate activation tensors stored in RAM and shared between succeeding layers reduce as well. The reason why the relation is not perfectly linear is because our runtime library tries to re-use heap memory for several activation tensors. How good this strategy works and how much memory it can save depends on the topology of the DNN that it is applied to. We cannot observe a reduction in SRAM consumption for element-wise pruning. This is because we do not remove any elements during element-wise pruning. While CRS can compress the sparse parameter tensors, it cannot change their original shapes. Therefore, as expected, no data dependencies are removed during decoding and as a result all intermediate activation tensors retain their original sizes.

D. Deployment Results

As the last step of evaluating our pipeline, we deployed several of the pruned and quantized models from our previous experiments on our target systems and monitored key runtime metrics. We especially focused on execution time per inference, power, and energy consumption. For measuring these metrics on our test systems, we used an *Agilent N6705A DC Power Analyzer* to provide them with a regulated

power supply. Furthermore, the Power Analyzer allowed us to measure the current and power drawn by the systems. To measure the execution time required for calculating the energy consumption of our DNN models, we used a GPIO signal. We toggled the signal every time an inference started and finished and monitored it using an oscilloscope. We present the results of our measurements for LeNet in Table III and the results for our other two DNN architectures in Table IV.

For the LeNet architecture, we used the models' accuracy on its evaluation dataset to compare the deployment of different pruning and quantization techniques. The logic behind this was that if models that were compressed using different approaches can achieve a similar accuracy, then they can be seen as direct alternatives and are therefore comparable. In our experimental setup we defined two relative accuracy boundaries for which we selected the smallest compressed models from our previous tests that meet them: >99% and >97%. In the second column of Table III we can see that LeNet can be compressed to well over 5% of its original parameter count while still passing both accuracy thresholds. We tested all selected models on our three target systems, including not only the pruned models but also their quantized counterparts, see the third and fourth columns. Note that using element pruning we were not able to deploy all selected models on the Arduino.

For all deployed LeNet models, we monitored execution time, power and energy consumption over a span of 8 different inferences. Their resulting averages are presented in the remaining columns of Table III. First, we see that the execution time per inference on the Pi 4B is significantly lower than on the Arduino or the Pi Pico. This is expected as the Pi 4B runs between 1.0 to 1.5 GHz while both the Arduino and the Pico run in a lower MHz range. When

TABLE IV

AVERAGE ($n = 8$) EXECUTION TIME, POWER AND ENERGY CONSUMPTION OBSERVED PER INFERENCE FOR ALEXNET AND RESNET. TO ACHIEVE DIFFERENT COMPRESSION RATES AND THUS DIFFERENT ACCURACY SCORES, WE USED L1-NORM STRUCTURAL PRUNING. IN ADDITION, WE USED POST TRAINING QUANTIZATION FOR ALL NON FLOATING-POINT MEASUREMENTS.

(a) AlexNet, CIFAR10, baseline accuracy $\approx 86\%$ for both float and uint8						
compression	type	rel. accuracy	system	execution time (ms)	power (mW)	energy (mWs)
95.9%	float	97.79%	arduino	—	—	—
			pico	—	—	—
			pi4b	6.60 ± 1.85	3795.81 ± 334.67	24.43 ± 4.10
-----	uint8	97.56%	arduino	—	—	—
			pico	1766.58 ± 0.25	92.40 ± 0.03	163.23 ± 0.07
			pi4b	3.96 ± 1.12	3809.41 ± 250.59	14.82 ± 2.71
98.2%	float	94.88%	arduino	—	—	—
			pico	—	—	—
			pi4b	2.68 ± 0.70	3687.37 ± 221.25	9.71 ± 1.76
-----	uint8	94.65%	arduino	403.11 ± 0.16	139.96 ± 0.17	56.42 ± 0.07
			pico	669.97 ± 0.19	86.41 ± 0.02	57.89 ± 0.03
			pi4b	2.93 ± 0.41	4187.75 ± 89.73	12.28 ± 2.05
99.6%	float	83.26%	arduino	252.40 ± 0.40	107.83 ± 0.42	27.22 ± 0.10
			pico	1435.42 ± 0.34	81.55 ± 0.07	117.06 ± 0.09
			pi4b	2.45 ± 0.09	4182.59 ± 66.35	10.25 ± 0.35
-----	uint8	82.33%	arduino	110.00 ± 0.01	141.17 ± 0.04	15.53 ± 0.01
			pico	186.57 ± 0.12	86.86 ± 0.21	16.21 ± 0.04
			pi4b	2.10 ± 0.14	4134.21 ± 52.03	8.68 ± 0.60
(b) ResNet, CIFAR10, baseline accuracy $\approx 85\%$ for float and $\approx 84\%$ for uint8						
compression	type	rel. accuracy	system	execution time (ms)	power (mW)	energy (mWs)
93.2%	float	96.25%	arduino	—	—	—
			pico	—	—	—
			pi4b	29.41 ± 2.62	4234.81 ± 121.13	124.24 ± 7.11
-----	uint8	96.43%	arduino	11983.40 ± 2.05	143.74 ± 0.49	1722.48 ± 5.69
			pico	25997.20 ± 4.00	91.94 ± 0.01	2390.24 ± 0.41
			pi4b	21.32 ± 3.32	4085.92 ± 213.90	86.54 ± 9.62
98.7%	float	92.50%	arduino	6105.20 ± 1.60	105.76 ± 1.85	645.69 ± 11.16
			pico	46266.50 ± 16.82	85.78 ± 0.02	3968.83 ± 1.49
			pi4b	9.41 ± 4.27	4536.99 ± 183.46	42.06 ± 16.53
-----	uint8	88.52%	arduino	2425.50 ± 0.92	102.38 ± 1.10	248.31 ± 2.70
			pico	4269.78 ± 2.58	87.81 ± 0.04	374.92 ± 0.36
			pi4b	7.74 ± 2.78	3863.07 ± 427.70	28.82 ± 6.98
99.6%	float	83.48%	arduino	1754.75 ± 0.31	106.57 ± 2.64	187.00 ± 4.63
			pico	11140.25 ± 1.85	83.13 ± 0.24	926.12 ± 2.61
			pi4b	5.42 ± 1.66	3560.66 ± 421.12	18.70 ± 4.01
-----	uint8	78.28%	arduino	806.80 ± 0.60	104.48 ± 0.09	84.29 ± 0.13
			pico	1214.53 ± 1.00	84.13 ± 0.06	102.18 ± 0.10
			pi4b	3.45 ± 0.22	3881.06 ± 72.77	13.37 ± 0.60

comparing the Raspberry Pi Pico and the Arduino Nano we observed a higher execution time on the Pico than on the Arduino (consistently). This is even though the Arduino runs with a clock speed only around half as fast as the Pico. On both systems the quantized models always outperformed their floating-point counter parts although much more pronounced on the Pico. This can be explained by the features present on both systems. First, the Arduino’s Cortex-M4 processor implements a real floating point unit while on the Pi Pico’s Cortex-M0+ processor floating point arithmetic has to be simulated. Second, the Arduino’s Cortex-M4 processor supports ARM’s Digital Signal Processing (DSP) extension giving it access to a subset of SIMD instructions to accelerate its integer operations. The Pi Pico does not implement the DSP extension.

Considering the power measured during inference for all deployed models, we see that all our tested systems on average draw a constant amount of power while we see a more

significant variation in the different samples taken for each model on the Pi 4B (note that the power consumption is much higher than on the other two systems). On the Arduino, the measured power consumption was between 100 to 150 mW on average while on the Pi Pico it was around 80 mW. In contrast to that, the Pi 4B generally consumed around 4W. However, in addition to power, execution time is the second factor in calculating a system’s energy consumption. Looking at the results, we see that for some cases the Pi 4B scored the best energy consumption per inference. It is often followed by the Arduino and then the Pi Pico. This is in reverse to the power consumption and shows that having an excellent runtime can compensate for high power consumption.

Besides LeNet, we also deployed our AlexNet and ResNet architectures, see Table IV. For both architectures we evaluated models which were compressed using structural pruning. This is different from our LeNet experiments where we tested both

structural and element-wise pruning. The reason we did not do this for AlexNet and ResNet is due to memory limitations on our Arduino and Pi Pico target systems, which made it impossible for us to deploy any element pruned models. For structural pruning the situation is different and we were able to feasibly deploy models. However, we were still forced to select models trained with aggressive compression rates that removed well over 90% of the original parameters. As a consequence we had to accept decreases in accuracy to be able to deploy models, see the third column of Tables IV(a) and IV(b).

To measure execution time, power, and energy consumption, we used the same approach as before. We again monitored all three metrics over 8 different inferences and calculated their averages and respective standard deviations. When looking at the results for AlexNet and ResNet, we see the same patterns we discussed for LeNet in Table III.

Yet we evaluated the two architectures as a way to explore upper boundaries of feasible DNN deployment. AlexNet features a very high number of trainable parameters while ResNet contains a high number of large and computationally expensive 2D-convolutions. This affects the deployment of the two architectures differently. While for AlexNet, we need to apply high compression rates to shrink the model size far enough to fit it into the memory of our target microcontrollers (see Sec. V-C) for ResNet execution time is the primary bottleneck. Even after pruning almost 99% of ResNet's parameters we still measure inference times of around 4 seconds on the Pi Pico, and of around 6 seconds on the Arduino Nano even when applying quantization, see the fifth column of Table IV(b). Only after removing >99% of all parameters the execution time ended up in an acceptable range (of around 1 second) on both microcontroller targets. However, these extremely high compression rates were accompanied by a high loss in accuracy, see the first column. This may make the usage of such a complex DNN architecture impractical for microcontroller targets. Therefore, we conclude that not only a model's parameter count but also its topology decides if it is deployable on a target system from a performance standpoint.

VI. DISCUSSION OF RESULTS

By using our compression and deployment pipeline, we were able to automatically and feasibly deploy DNNs to microcontrollers. Compressing DNNs allowed us to achieve significant savings in memory consumption, execution time, and energy consumption at runtime, without sacrificing model accuracy for it. For pruning, we achieved the best results and most savings with structural pruning. When comparing different pruning strategies, our experiments indicate that structural pruning offers better opportunities for saving memory and execution time than element-wise pruning. In addition, the execution of DNNs that were compressed using this technique did not require any special support for sparse matrix formats as it is required for element pruning. Furthermore, we observed that for structural pruning, using different state-of-the-art heuristics did not have that much of an impact. Choosing a reasonable pruning schedule and allowing for retraining has proven to be more effective. Additionally, applying weight quantization

together with structural pruning resulted in even more savings not only in memory consumption, but also in execution time. This is due to the fact that our target systems were able to process much more efficiently in integer- than in floating-point space. Besides that, we noticed that our different compression and deployment strategies had almost no influence on the power drawn by both the Pi Pico and the Arduino during inference. This means that the observed energy savings were mainly the result of execution times.

We come to the conclusion that a DNN model is deployed optimally on a microcontroller, if it runs on a system where it fits into the available memory and draws the least amount of power under load while still being able to run inferences in a reasonable time frame. Furthermore, we argue that a DNN's execution time has to be seen in relation to the frequency at which input samples are generated by connected sensors.

VII. CONCLUSION

In this work we presented a configurable pipeline for compressing DNNs and deploying them on Cortex-M based microcontrollers. To achieve compression, our pipeline utilizes network pruning and weight quantization techniques. The deployment is handled by using a proposed runtime environment, which consists of a code generator for mapping trained networks to executable C-code and a runtime library which provides optimized implementations of common DNN layers. We used the introduced pipeline to compare DNNs compressed with different pruning and quantization techniques. Furthermore, we tested how compression influences runtime performance on multiple target systems. We were able to show that even larger DNN architectures like AlexNet or ResNet can be feasibly deployed on microcontrollers featuring memory footprints of as little as 1-2 MB Flash and 256 Kb SRAM while still achieving good execution time and accuracy results.

ACKNOWLEDGEMENT

This work was supported by the Bavarian Ministry for Economic Affairs, Infrastructure, Transport and Technology through the Center for Analytics-Data-Applications (ADA-Center) within the framework of "BAYERN DIGITAL II".

REFERENCES

- [1] S. Hershey, S. Chaudhuri, D. P. W. Ellis, J. F. Gemmeke, A. Jansen, R. C. Moore, M. Plakal, D. Platt, R. A. Saurous, B. Seybold, M. Slaney, R. J. Weiss, and K. Wilson, "CNN architectures for large-scale audio classification," in *2017 IEEE International Conference on Acoustics, Speech and Signal Processing (ICASSP)*, Mar. 2017, pp. 131–135.
- [2] O. Abdel-Hamid, A.-r. Mohamed, H. Jiang, L. Deng, G. Penn, and D. Yu, "Convolutional Neural Networks for Speech Recognition," *IEEE/ACM Transactions on Audio, Speech, and Language Processing*, vol. 22, no. 10, pp. 1533–1545, Oct. 2014.
- [3] K. He, X. Zhang, S. Ren, and J. Sun, "Deep Residual Learning for Image Recognition," in *2016 IEEE Conference on Computer Vision and Pattern Recognition (CVPR)*, Jun. 2016, pp. 770–778.
- [4] A. Krizhevsky, "Learning Multiple Layers of Features from Tiny Images," *University of Toronto*, May 2012.
- [5] T. Kautz, B. H. Groh, J. Hannink, U. Jensen, H. Strubberg, and B. M. Eskofier, "Activity recognition in beach volleyball using a Deep Convolutional Neural Network," *Data Mining and Knowledge Discovery*, vol. 31, no. 6, pp. 1678–1705, Nov. 2017.

- [6] V. Sze, Y.-H. Chen, T.-J. Yang, and J. S. Emer, "Efficient Processing of Deep Neural Networks: A Tutorial and Survey," *Proceedings of the IEEE*, vol. 105, no. 12, pp. 2295–2329, Dec. 2017.
- [7] A. Canziani, A. Paszke, and E. Culurciello, "An Analysis of Deep Neural Network Models for Practical Applications," *arXiv:1605.07678 [cs]*, Apr. 2017.
- [8] N. D. Lane, S. Bhattacharya, A. Mathur, P. Georgiev, C. Forlivesi, and F. Kawsar, "Squeezing Deep Learning into Mobile and Embedded Devices," *IEEE Pervasive Computing*, vol. 16, no. 3, pp. 82–88, 2017.
- [9] Y. L. Cun, J. S. Denker, and S. A. Solla, "Optimal Brain Damage," in *Advances in Neural Information Processing Systems*. Morgan Kaufmann, 1990, pp. 598–605.
- [10] B. Jacob, S. Kligys, B. Chen, M. Zhu, M. Tang, A. Howard, H. Adam, and D. Kalenichenko, "Quantization and training of neural networks for efficient integer-arithmetic-only inference," in *Proceedings of the IEEE Conference on Computer Vision and Pattern Recognition (CVPR)*, Jun. 2018.
- [11] M. Nagel, R. A. Amjad, M. V. Baalen, C. Louizos, and T. Blankevoort, "Up or Down? Adaptive Rounding for Post-Training Quantization," in *International Conference on Machine Learning*. PMLR, Nov. 2020, pp. 7197–7206.
- [12] C. Liu, J. Li, and Y. Gong, "SVD-based universal DNN modeling for multiple scenarios," in *Sixteenth Annual Conference of the International Speech Communication Association*, 2015.
- [13] S. Han, H. Mao, and W. J. Dally, "Deep compression: Compressing deep neural networks with pruning, trained quantization and Huffman coding," *International Conference on Learning Representations (ICLR)*, 2016.
- [14] H. Li, A. Kadav, I. Durdanovic, H. Samet, and H. P. Graf, "Pruning Filters for Efficient ConvNets," *arXiv:1608.08710 [cs]*, Mar. 2017.
- [15] S. Anwar, K. Hwang, and W. Sung, "Structured pruning of deep convolutional neural networks," *J. Emerg. Technol. Comput. Syst.*, vol. 13, no. 3, Feb. 2017.
- [16] R. Barrett, M. Berry, T. F. Chan, J. Demmel, J. Donato, J. Dongarra, V. Eijkhout, R. Pozo, C. Romine, and H. V. d. Vorst, *Templates for the Solution of Linear Systems: Building Blocks for Iterative Methods, 2nd Edition*. Philadelphia, PA: SIAM, 1994.
- [17] A. Krizhevsky, I. Sutskever, and G. E. Hinton, "ImageNet classification with deep convolutional neural networks," *Communications of the ACM*, vol. 60, no. 6, pp. 84–90, May 2017.
- [18] Y. LeCun, B. Boser, J. S. Denker, D. Henderson, R. E. Howard, W. Hubbard, and L. D. Jackel, "Backpropagation Applied to Handwritten Zip Code Recognition," *Neural Computation*, vol. 1, no. 4, pp. 541–551, Dec. 1989.
- [19] P. Hu, X. Peng, H. Zhu, M. M. S. Aly, and J. Lin, "OPQ: Compressing Deep Neural Networks with One-shot Pruning-Quantization," *Proceedings of the AAAI Conference on Artificial Intelligence*, vol. 35, May 2021.
- [20] Z. Liu, M. Sun, T. Zhou, G. Huang, and T. Darrell, "Rethinking the value of network pruning," in *International Conference on Learning Representations*, 2019.
- [21] B. Reddy, Y.-H. Kim, S. Yun, C. Seo, and J. Jang, "Real-Time Driver Drowsiness Detection for Embedded System Using Model Compression of Deep Neural Networks," in *2017 IEEE Conference on Computer Vision and Pattern Recognition Workshops (CVPRW)*, Jul. 2017, pp. 438–445.
- [22] S. Lu, G. Qian, Q. He, F. Liu, Y. Liu, and Q. Wang, "In Situ Motor Fault Diagnosis Using Enhanced Convolutional Neural Network in an Embedded System," *IEEE Sensors Journal*, vol. 20, no. 15, pp. 8287–8296, Aug. 2020.
- [23] J. Lin, W.-M. Chen, Y. Lin, j. cohn, C. Gan, and S. Han, "MCUNet: Tiny Deep Learning on IoT Devices," in *Advances in Neural Information Processing Systems*, vol. 33. Curran Associates, Inc., 2020, pp. 11 711–11 722.
- [24] B. Zoph and Q. V. Le, "Neural Architecture Search with Reinforcement Learning," *arXiv, Tech. Rep.*, Feb. 2017.
- [25] R. David, J. Duke, A. Jain, V. J. Reddi, N. Jeffries, J. Li, N. Kreeger, I. Nappier, M. Natraj, S. Regev, R. Rhodes, T. Wang, and P. Warden, "TensorFlow Lite Micro: Embedded Machine Learning on TinyML Systems," *arXiv:2010.08678 [cs]*, Mar. 2021.
- [26] T. Akiba, S. Sano, T. Yanase, T. Ohta, and M. Koyama, "Optuna: A next-generation hyperparameter optimization framework," in *Proceedings of the 25th ACM SIGKDD International Conference on Knowledge Discovery & Data Mining*, ser. KDD '19. New York, NY, USA: Association for Computing Machinery, 2019, p. 2623–2631.
- [27] S. J. Hanson and L. Y. Pratt, "Comparing biases for minimal network construction with back-propagation," in *Proceedings of the 1st International Conference on Neural Information Processing Systems*. Cambridge, MA, USA: MIT Press, Jan. 1988, pp. 177–185.
- [28] P. Molchanov, S. Tyree, T. Karras, T. Aila, and J. Kautz, "Pruning Convolutional Neural Networks for Resource Efficient Inference," *arXiv:1611.06440 [cs]*, Jun. 2017.
- [29] S. Han, J. Pool, J. Tran, and W. J. Dally, "Learning both weights and connections for efficient neural networks," in *Proceedings of the 28th International Conference on Neural Information Processing Systems - Volume 1*, ser. NIPS'15. Cambridge, MA, USA: MIT Press, 2015, p. 1135–1143.
- [30] H. Hu, R. Peng, Y.-W. Tai, and C.-K. Tang, "Network Trimming: A Data-Driven Neuron Pruning Approach towards Efficient Deep Architectures," *arXiv:1607.03250 [cs]*, Jul. 2016.
- [31] M. Zhu and S. Gupta, "To prune, or not to prune: exploring the efficacy of pruning for model compression," *arXiv:1710.01878 [cs, stat]*, Nov. 2017.
- [32] O. R. developers, "ONNX Runtime," <https://onnxruntime.ai/>, 2021, version: 1.8.0.
- [33] I. Hubara, Y. Nahshan, Y. Hanani, R. Banner, and D. Soudry, "Improving Post Training Neural Quantization: Layer-wise Calibration and Integer Programming," *arXiv:2006.10518 [cs, stat]*, Dec. 2020.
- [34] Y. LeCun, C. Cortes, and C. Burges, "MNIST handwritten digit database," *ATT Labs [Online]*. Available: <http://yann.lecun.com/exdb/mnist>, vol. 2, 2010.